

Augmented projections for ptychographic imaging

Stefano Marchesini and Andre Schirotzek

*Advanced Light Source, Lawrence Berkeley National Laboratory, Berkeley, CA 94720**

Chao Yang

Computational Research Division, Lawrence Berkeley National Laboratory, Berkeley, CA 94720.†

Filipe Maia

NERSC, Lawrence Berkeley National Laboratory, Berkeley, CA 94720‡

Ptychography is a popular technique to achieve diffraction limited resolution images of a two or three dimensional sample using high frame rate detectors. We introduce a relaxation of common projection algorithms to account for instabilities given by intensity and background fluctuations, position errors, or poor calibration using multiplexing illumination. This relaxation introduces an additional phasing optimization at every step that enhances the convergence rate of common projection algorithms. Numerical tests exhibit the exact recovery of the object and the noise when there is high redundancy in the data.

I. INTRODUCTION

In a ptychography experiment¹⁻⁶ (see Fig. 1), a two dimensional small beam with distribution $w(\mathbf{r})$ of dimension $m \times m$ illuminates an unknown object of interest $\hat{\psi}(\mathbf{r} + \mathbf{x}_{(i)})$, where $\mathbf{x}_{(i)}$ is used to denote the location of the subregion. For simplicity we consider square matrices, generalization to non-square matrices is straightforward but requires more indices and complicates notation. We assume that a sequence of k diffraction images $a_{(i)}^2(\mathbf{q})$ are collected as the position $\mathbf{x}_{(i)}$ of the object is rastered. Each frame $a_{(i)}$ contains $m \times m$ pixels. We consider the case in which $a_{(i)}$ is the magnitude of the discrete two dimensional discrete Fourier transform (DFT) of the unknown object. If we let \mathcal{F} be a 2D DFT operator, the relationship among $a_{(i)}$, $w(\mathbf{r})$ and $\hat{\psi}(\mathbf{r} + \mathbf{x}_{(i)})$ can be expressed as follows:

$$\begin{aligned} a_{(i)}(\mathbf{q}) &= \left| \mathcal{F}w(\mathbf{r})\hat{\psi}(\mathbf{r} + \mathbf{x}_{(i)}) \right|, & (1) \\ \mathbf{r} &= r\mathbf{m}, \mathbf{q} = \frac{2\pi}{r}\mathbf{m} \\ \mathcal{F}f &= \sum_{\mathbf{r}} e^{i\mathbf{q}\cdot\mathbf{r}} f(\mathbf{r}), \\ \mathbf{m} &= (\mu, \nu), \quad \mu, \nu = (0 \dots m - 1), \end{aligned}$$

where r is a lengthscale, and the sum over \mathbf{r} is given on all the indices $m \times m$ of \mathbf{r} .

As \mathbf{x} is rastered on a typically coarser grid, $\mathbf{r} + \mathbf{x}$ spans a finer grid of dimension $n \times n$, where $n > m$. We denote with subindex $i = (1 \dots k)$ the sequence of raster points $\mathbf{x}_{(i)}$.

We introduce the illumination operator $Q_{(i)}$ associated with translation $x_{(i)}$ that extracts a frame out of $\hat{\psi}$, and scales the frame point-wise by the illumination function $w(\mathbf{r})$: (see Fig. 1)

$$\begin{aligned} \hat{z}_{(i)}(\mathbf{r}) &= w(\mathbf{r})\hat{\psi}(\mathbf{r} + \mathbf{x}_{(i)}) = Q_{(i)}(\mathbf{r})\hat{\psi}, \\ Q_{(i)}(\mathbf{r}) &= w(\mathbf{r})e^{i\mathbf{x}_{(i)}\cdot\mathbf{r}}. \end{aligned}$$

where $z_{(i)}$ represents the frames extracted from ψ and multiplied by the probe $w(\mathbf{r})$.

Using linear algebra notation, we represent $\hat{\psi}$ as a vector of length n^2 , $\hat{\psi} \in \mathbb{C}^{n^2}$. The moving beam associated with the illumination function $w(\mathbf{r})$ can be represented as an $m^2 \times n^2$ sparse ‘‘illumination matrix’’ $Q_{(i)}$ ($i = 1, 2, \dots, k$).

The relationship between the diffraction measurements collected in a ptychography experiment and the unknown object to be recovered can be represented compactly as:

$$\mathbf{a} = |\mathbf{F}\mathbf{Q}\hat{\psi}|, \quad (2)$$

if we stack the diffraction measurements $a_{(i)}$ into a long vector \mathbf{a} , and define various matrices as follows:

$$\begin{aligned} \mathbf{a} &= \begin{pmatrix} a_1 \\ \vdots \\ a_k \end{pmatrix}, \quad \mathbf{Q} = \begin{pmatrix} Q_1 \\ \vdots \\ Q_k \end{pmatrix}, \\ \hat{\mathbf{z}} &= \begin{pmatrix} \hat{z}_1 \\ \vdots \\ \hat{z}_k \end{pmatrix}, \quad \mathbf{F} = \begin{pmatrix} \mathcal{F} & & \\ & \ddots & \\ & & \mathcal{F} \end{pmatrix}. \end{aligned}$$

The objective of the ptychographic reconstruction problem is to find $\hat{\psi}$ given \mathbf{a} from (Eq. 2). This is often formulated using a ‘‘divide and conquer’’ approach referred to as *projection algorithms*, *iterative transform methods*, or *alternating direction methods*⁷. One formulates the relationship (Eq. 2) as:

$$\mathbf{a} = |\mathbf{F}\hat{\mathbf{z}}|, \quad (3)$$

$$\hat{\mathbf{z}} = \mathbf{Q}\hat{\psi}. \quad (4)$$

These algorithms are often defined in terms of two projection operators P_F and P_Q that project onto the solution z to Eqs. 3 and 4 that is closest to the current estimate described in Section II.

Alternative approaches include formulating the problem as:

$$\min_{\hat{\psi}} \|\mathbf{a} - |\mathbf{F}\mathbf{Q}\hat{\psi}|\|$$

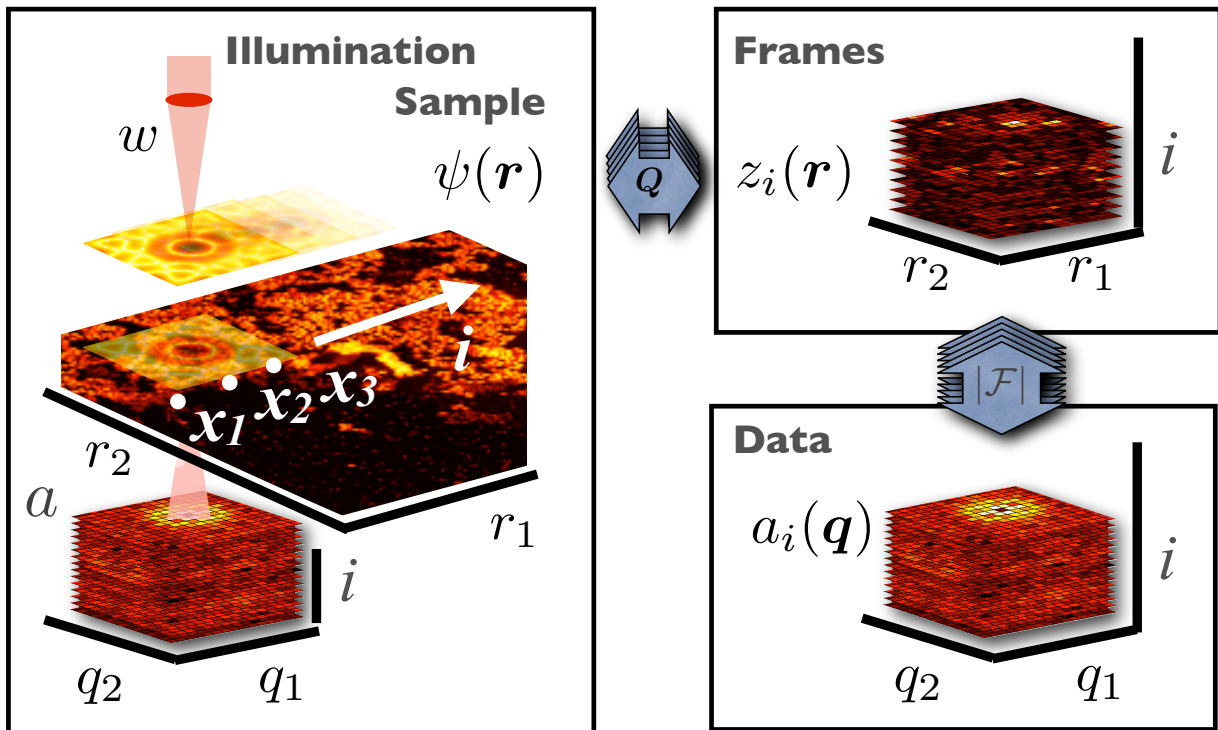


FIG. 1: (Left) Experimental geometry in ptychography: An unknown sample with transmission $\psi(\mathbf{r})$ is rastered through an illuminating beam $w(\mathbf{r})$, and a sequence of diffraction measurements $|a_{(i)}|^2$ is recorded on an area detector as the sample is rastered around. The point-wise product between illuminating function and sample $z_{(i)}(\mathbf{r}) = w(\mathbf{r})\psi(\mathbf{r} + \mathbf{x}_i)$ is related to the measurement by a Fourier magnitude relationship $a_{(i)}(\mathbf{q}) = |\mathcal{F}z_{(i)}|$.

and solve by standard unconstrained minimization algorithms such as projected gradient, conjugate gradient, Newton and quasi-Newton methods^{8,9}. Another approach proposes a convex relaxation of the quadratic problem by lifting to an $n^2 \times n^2$ space¹⁰⁻¹².

In the following section II we will describe the standard operators commonly used in the literature. In section III we will introduce an intermediate variable $c_{(i)}$, to account for intensity fluctuations, replacing Eq. (4) with $c_{(i)}z_{(i)} = Q_{(i)}\psi$, $i = (1, \dots, k)$. In section IV we extend this approach to situations in which intensity data is added incoherently or multiplexed. In section V we extend this approach to situations in which the data is corrupted by position errors. In Section VI we introduce an unknown background $b(\mathbf{q})$, different for every pixel, but constant throughout the acquisition (or $b_{(i)}$ different for every frame i , but constant throughout each frame). In Section VII we report the following numerical results:

- Exact reconstruction with intensity fluctuation given by the coefficients $c_{(i)}$ (see Fig. 4).
- Accelerated convergence (Fig. 5) even when no intensity fluctuation is present in the data by using only the phase of $c_{(i)}$ (Table II)
- Exact reconstruction with multiplexing using 4 si-

multaneous illuminations adding incoherently on the detector, with perturbation of the amplitudes (Fig. 6)

- Exact reconstruction of fluctuating background noise independent from the sample (Figs. 8,9).
- Position recovery (Figs. 7) of the illuminating probe using iterative Taylor expansion optimization.

II. STANDARD PROJECTION ALGORITHMS

The projection operator P_F mentioned in the previous section is often known as the *Fourier magnitude* projection operator. Applying this operator to a vector \mathbf{z} yields

$$P_F^a \mathbf{z} = \mathbf{F}^* \frac{\mathbf{Fz}}{|\mathbf{Fz}|} \cdot \mathbf{a}. \quad (5)$$

where division and product are intended as element-wise operations. It is easy to verify that $|P_F^a \mathbf{z}| = |\mathbf{a}|$ and therefore $P_F \mathbf{z}$ satisfies Eq. (3) for any \mathbf{z} . P_F is a projection

in the sense that

$$P_F^a \mathbf{z} = \arg \min_{\bar{\mathbf{z}}} \|\mathbf{z}_{(i)} - \bar{\mathbf{z}}_{(i)}\|, \quad (6)$$

subject to $|\mathbf{F}\bar{\mathbf{z}}| = \mathbf{a}$,

where $\|\cdot\|$ denotes the Euclidean norm. The matrix \mathbf{Q} defines an orthogonal projection operator P_Q that projects any vector in \mathbb{C}^{km^2} onto the range of \mathbf{Q} :

$$P_Q = \mathbf{Q}(\mathbf{Q}^*\mathbf{Q})^{-1}\mathbf{Q}^*, \quad (7)$$

In the simple alternating projection algorithm, the approximation to the solutions of (4) and (7) are updated by:

$$\begin{aligned} \mathbf{z}^{(\ell+1)} &= [P_Q P_F] \mathbf{z}^{(\ell)} \\ \psi^{(\ell+1)} &= (\mathbf{Q}^*\mathbf{Q})^{-1}\mathbf{Q}^* \mathbf{z}^{(\ell+1)}. \end{aligned}$$

Here $\psi^{(\ell)}$ is the running estimate of $\hat{\psi}$ that solves the linear subproblem:

$$\psi^{(\ell)} = \arg \min_{\psi} \|\mathbf{z}^{(\ell)} - \mathbf{Q}\psi\|, \quad (8)$$

One may also introduce a regularization factor ϵ and update the running estimate as:

$$\psi^{(\ell+1)} = (\mathbf{Q}^*\mathbf{Q} + \epsilon)^{-1}\mathbf{Q}^* \left(\mathbf{z}^{(\ell+1)} + \epsilon\psi^{(\ell)} \right).$$

with typically $\psi^{(0)} = 0$. The projection operator P_Q can be expressed in terms of the solution to Eq. 8:

$$P_Q \mathbf{z}^{(\ell)} = \mathbf{Q}(\mathbf{Q}^*\mathbf{Q})^{-1}\mathbf{Q}^* \mathbf{z}^{(\ell)} = \mathbf{Q}\psi^{(\ell)}.$$

$(\mathbf{Q}^*\mathbf{Q})^{-1}$ is a normalization factor corresponding to the sum of all the intensities of the illumination function. \mathbf{Q}^* is the operator that scales all the frames $z_{(i)}$ by the conjugate of the probe $w^*(\mathbf{r})$ and translates them by $-\mathbf{x}_{(i)}$ onto the image ψ :

$$\mathbf{Q}^* \mathbf{z} = \sum_i e^{-i\mathbf{x}_{(i)} \cdot \partial_{\mathbf{r}}} w^*(\mathbf{r}) z_{(i)}(\mathbf{r})$$

A number of heuristic algorithms has been proposed^{13,14}, a few examples are given in Tab. I, with $\beta \in [0, 1]$ is a relaxation parameter. Very recently, an alternating direction method (ADM) designed to work with a special augmented Lagrangian function⁷. This function is minimized by applying a block coordinate descent scheme (or alternating search directions) akin to these projection operators.

III. FLUCTUATING INTENSITIES, AND AUGMENTED PHASE RETRIEVAL

One of the practical issues one may face in ptychography is the intensity fluctuation among different diffraction frames introduced by instabilities in the light source, optics and shutters. Such fluctuation can be accounted

for by introducing a scaling factor $c_i \in \mathbb{C}$ for each diffraction frame. By allowing c_i to be complex, we introduce an optimization of the relative phase between frames. As a result, the definition \hat{z}_i is modified so that the equation

$$c_i \hat{z}_i = Q_i \hat{\psi}, \quad (9)$$

holds for $i = 1, 2, \dots, k$. The phase of the scaling factor c_i is a relaxation parameter that enables us to improve the convergence of iterative algorithms. As we will see below, the phase of c enables us to find the intersection between P_F^a and P_Q more easily since a constant phase factor multiplying each frame is insensitive to the Fourier magnitude projection. By optimizing the phase among each frame, we solve the phase at a resolution given by the step size between frames.

Since both c_i and $\hat{\psi}$ are unknown in (9), the solution to (9) is clearly not unique. To exclude the trivial solution $c_i = 0$, for $i = 1, 2, \dots, k$ and $\psi = 0$, we introduce an additional constraint and solve

$$\begin{aligned} (\psi_{\min}, c_{(i)}) &= \arg \min_{\psi, c_{(i)}} \sum_i |Q_{(i)}\psi - c_{(i)}z_{(i)}|^2 \quad (10) \\ &\text{subject to } \sum c_{(i)} = \gamma \end{aligned}$$

We can also eliminate ψ and solve the following problem:

$$\arg \min_{c, \lambda} \|(I - P_Q)\text{Diag}(c) \mathbf{z}\|^2 + \lambda \left(\sum c_i - k \right)$$

Since it is sufficient to determine the relative difference among different c_i 's, the choice of γ is arbitrary. A reasonable choice is $\gamma = k$. We can show (see the Appendix) that

$$\mathbf{c} = \alpha H \setminus \mathbf{1}, \quad \mathbf{c} = \begin{pmatrix} c_1 \\ \vdots \\ c_k \end{pmatrix} \quad \mathbf{1} = \begin{pmatrix} 1 \\ \vdots \\ 1 \end{pmatrix}, \quad (11)$$

where α is chosen to ensure that $\sum_{i=1}^k c_i = k$ holds, and the matrix H is given by:

$$\begin{aligned} H_{i,j} &= z_{(i)}^* \left(\delta_{i,j} I - (P_Q)_{i,j} \right) z_{(j)}, \quad (12) \\ (P_Q)_{i,j} &= \mathbf{Q}_i \frac{1}{\mathbf{Q}^* \mathbf{Q}} \mathbf{Q}_j^* \end{aligned}$$

Once \mathbf{c} is available, the least squares approximation to ψ can be written as

$$\psi = (\mathbf{Q}^*\mathbf{Q})^{-1} \mathbf{Q}^* D_{\mathbf{c}} \mathbf{z}, \quad D_{\mathbf{c}} = \begin{pmatrix} c_1 I & & \\ & \ddots & \\ & & c_k I \end{pmatrix}.$$

To modify projection algorithms to account for intensity fluctuations, we replace the operator P_Q used in the standard projection algorithms listed in Table I by an augmented projection operator P_Q^c defined as:

$$P_Q^c = D_{\mathbf{c}}^{-1} P_Q D_{\mathbf{c}}.$$

projection algorithm	updating formula $\mathbf{z}^{(\ell+1)} =$
Alternating Projection ¹⁵	$[P_Q P_F] \mathbf{z}^{(\ell)}$
HIO ¹⁵	$[P_Q P_F + (I - P_Q)(I - \beta P_F)] \mathbf{z}^{(\ell)}$
Difference Map ⁵	$[P_F P_Q + (I - P_F)(I - \beta P_Q)] \mathbf{z}^{(\ell)}$
RAAR ¹⁴	$[2\beta P_Q P_F + (1 - 2\beta)P_F + \beta(P_Q - I)] \mathbf{z}^{(\ell)}$

TABLE I: Popular fix-point algorithms used in phase retrieval

An alternative modification is to redefine the probe as $\mathbf{Q}_c = D_c^{-1} \mathbf{Q}$ by incorporating the scaling factors c_i , and write:

$$P_{\mathbf{Q}}^c = \mathbf{Q}_c (\mathbf{Q}_c^* \mathbf{Q}_c)^{-1} \mathbf{Q}_c^*$$

Although the construction of $P_{\mathbf{Q}}^c$ is motivated by the need to account for intensity fluctuations among different diffraction frames in the measured data, it turns out to be a useful technique for accelerating the convergence of projection algorithms even when no intensity fluctuation is present in the data. This is because we perform an additional phasing optimization around the P_Q projection that is invisible to the Fourier magnitude projection. This enables the intersection between the constraints associated with these P_F^a and $P_{\mathbf{Q}}^c$ to be detected more easily.

IV. MULTIPLEXING AND INCOHERENT MEASUREMENTS

A practical issue in ptychography are the strict requirements of the experimental geometry to achieve high quality data. For example the need for stable, coherent illumination of the sample, careful control of vibrations, and limited detector response function all contribute to limit the specifications of a ptychographic microscope. Here we consider the case of multiplexing incoherent measurements to relax some of the experimental constraint. The sum of intensities, rather than amplitudes is a result of the incoherent addition with varying experimental parameters during the measurement. By relaxing the model of the measurement process and solving the optimization problem described in the previous section, we attempt to recover unknown instantaneous fluctuations of the parameters and improve convergence.

The measurement model is as follows:

$$a_{(i)} = \sqrt{\sum_{\iota} \Omega_{i,\iota} |\mathcal{F} \hat{z}_{(\iota)}|^2} \quad (13)$$

where Ω is a sparse matrix that represents an averaging operation of the intensities. For example, a single exposure may represent the sum of the intensities generated by an illumination beam that translates during the exposure, or may represent a binned version of the high dimensional signal. We consider z_i the highly redundant set of frames generated for all the positions of

the illumination function during an exposure. More efficient parameterization of the data are also applicable, (see next section). The operator Ω then simply adds the intensity of the frames associated with an exposure.

The projection operator associated with this problem can be written as follows:

$$P_F^{a,\Omega} \tilde{z} = \tilde{z} \sqrt{\Omega^* \frac{a_{(i)}^2}{\Omega |\tilde{z}_{(i)}|^2}}$$

where Ω^* is an operator that copies the entries over all the frames that contribute to an exposure. Replacing this operator in the reconstruction process is subject of recent interest by several groups¹⁶.

However, since fluctuations about an average are unconstrained by the measurement, P_F is insensitive to modifications of the relative amplitude of the frames. We can achieve higher performance if we optimize the relative amplitude and phases of the frames as described in the previous section.

Numerical tests described in section VII show the exact recovery (within numerical precision) of the object and a multiplexing array of beam positions averaged incoherently with errors in the calibration of the amplitude factors. The ability to recover the relative amplitude of a redundant set of frames that are averaged during the measurement enables us also to identify which instance of the experimental parameters occurred. The augmented projection described in the previous section attempts to do just what we need to recover or calibrate the amplitude coefficients of our multiplexing array.

V. POSITION ERRORS

We consider the case in which the probe w is translated from the input coordinate by an unknown distance ξ . We call \mathbf{Q}_ξ the unknown illumination matrix used to generate the data. To determine the illumination matrix, we determine the parameter ξ so that the error $\varepsilon_{\mathbf{Q}_\xi}$ is minimized:

$$\arg \min_{\xi} \left\| [I - P_{\mathbf{Q}_\xi}] \mathbf{z} \right\|^2 \quad (14)$$

We restrict initially to 1-dimensional translations. Given the illumination function w , we can compute the first and second order derivatives with respect to translation. We denote by Q_i, R_i, S_i the illumination matrices that extract a frame out of an image and multiplies by

$(w(\mathbf{x}), \partial_x w(\mathbf{x}), \partial_x^2 w(\mathbf{x}))$ respectively. $\mathbf{Q}, \mathbf{R}, \mathbf{S}$ are tall and skinny matrices of the same size as \mathbf{Q} discussed earlier, with identical location of the non-zero entries. The probe is perturbed to second order as follows:

$$\mathbf{Q}_\xi = \mathbf{Q} + \xi \mathbf{R} + \xi^2 \mathbf{S}.$$

where ξ is diagonal and real, and represents the translation distance different for every frame i . When the translation ξ has two components, we write:

$$\xi = \begin{pmatrix} \xi_1 \\ \xi_2 \end{pmatrix} \quad \mathbf{R} = \begin{pmatrix} \mathbf{R}_1 \\ \mathbf{R}_2 \end{pmatrix} \quad \mathbf{S} = \begin{pmatrix} \mathbf{S}_{11} & \mathbf{S}_{12} \\ \mathbf{S}_{21} & \mathbf{S}_{22} \end{pmatrix}$$

where R_1, R_2, \dots, S_{22} are the illumination matrices that extract a frame out of an image and multiply by $(w(\mathbf{x}), \partial_{x_1} w(\mathbf{x}), \partial_{x_2} w(\mathbf{x}), \dots, \partial_{x_2}^2 w(\mathbf{x}))$ respectively. The second order term in the Taylor expansion becomes the sum over all dimensions:

$$\begin{aligned} \xi^2 \mathbf{S} &\rightarrow \xi_1^2 \mathbf{S}_{11} + 2\xi_1 \xi_2 \mathbf{S}_\times + \xi_2^2 \mathbf{S}_{22}. \\ \mathbf{S}_\times &\equiv \frac{1}{2} (\mathbf{S}_{12} + \mathbf{S}_{21}). \end{aligned}$$

Setting $\partial_{\xi_1}^* \|\cdot\|$ and $\partial_{\xi_2}^* \|\cdot\|$ to 0 gives (see appendix B):

$$\begin{pmatrix} H_1 & H_\times \\ H_\times & H_2 \end{pmatrix} \begin{pmatrix} \xi_1 \\ \xi_2 \end{pmatrix} = \begin{pmatrix} \mathbf{z}_i^* \mathbf{z}_{\mathbf{R}_1 i} + \mathbf{z}_{\mathbf{R}_1 i}^* \mathbf{z}_i \\ \mathbf{z}_i^* \mathbf{z}_{\mathbf{R}_2 i} + \mathbf{z}_{\mathbf{R}_2 i}^* \mathbf{z}_i \end{pmatrix}, \quad (15)$$

using the definition $\mathbf{z}_{\mathbf{R}_1, \dots, \mathbf{S}_{22}} \equiv [\mathbf{R}_1, \dots, \mathbf{S}_{22}] \frac{1}{\mathbf{Q}^* \mathbf{Q}} \mathbf{Q}^* \mathbf{z}$, $\mathbf{z} \equiv [I - P_{\mathbf{Q}}] \mathbf{z}$, and where the matrices $H_{1,2,\times}$ are defined as:

$$\begin{aligned} (H_1)_{ij} &= (\mathbf{z}_{\mathbf{R}_1 i}^* \mathbf{z}_{\mathbf{R}_1 i} - 2\mathbf{z}_i^* \mathbf{z}_{\mathbf{S}_{11} i}) \delta_{ij} - \mathbf{z}_i^* (O_{11})_{ij} \mathbf{z}_j + \text{cc}, \\ (H_2)_{ij} &= (\mathbf{z}_{\mathbf{R}_2 i}^* \mathbf{z}_{\mathbf{R}_2 i} - 2\mathbf{z}_i^* \mathbf{z}_{\mathbf{S}_{22} i}) \delta_{ij} - \mathbf{z}_i^* (O_{22})_{ij} \mathbf{z}_j + \text{cc}, \\ (H_\times)_{ij} &= (\mathbf{z}_{\mathbf{R}_1 i}^* \mathbf{z}_{\mathbf{R}_2 i} - 2\mathbf{z}_i^* \mathbf{z}_{\mathbf{S}_\times i}) \delta_{ij} - \mathbf{z}_i^* (O_\times)_{ij} \mathbf{z}_j + \text{cc}, \end{aligned}$$

where

$$\begin{aligned} (O_{11})_{ij} &\equiv (\mathbf{R}_1)_i \frac{1}{\mathbf{Q}^* \mathbf{Q}} (\mathbf{R}_1)_j^*, \\ (O_{22})_{ij} &\equiv (\mathbf{R}_2)_i \frac{1}{\mathbf{Q}^* \mathbf{Q}} (\mathbf{R}_2)_j^*, \\ (O_\times)_{ij} &\equiv (\mathbf{R}_1)_i \frac{1}{\mathbf{Q}^* \mathbf{Q}} (\mathbf{R}_2)_j^*. \end{aligned}$$

The system of equations can be solved efficiently by sparse linear algebra solvers. The entries of the equation are given by the dot product between frames $(\mathbf{z}, \mathbf{z}_{\mathbf{R}_1}, \dots, \mathbf{z}_{\mathbf{S}_{22}})$ with partial overlap and scaling factors given by $\mathbf{R}_{1,2}^* \frac{1}{\mathbf{Q}^* \mathbf{Q}} \mathbf{R}_{1,2}$. The terms $\mathbf{z} \mathbf{z} \mathbf{S}$ are higher order corrections close to the solution and can be neglected in practice. In Section VII we will show that this method can recover the position perturbations to numerical accuracy when the perturbations are a fraction than the probe width.

VI. BACKGROUND NOISE

Here we consider an unknown offset $b(\mathbf{q})$ (background) different for every pixel but constant throughout the acquisition:

$$|\tilde{z}_{(i)}|^2 + b = a_{(i)}^2, \quad \tilde{z}_{(i)} = \mathcal{F}z_{(i)}. \quad (16)$$

A trivial variation of the problem is when $b_{(i)}(\mathbf{q})$ is different for every frame but the same for every pixel \mathbf{q} .

At each iteration, we solve the following *offset* minimization problem with an additional scaling parameter:

$$\begin{aligned} \min_{b, \eta} \sum_i \left| |\tilde{z}_{(i)}|^2 - |\tilde{z}_{(i)}^{(\ell)}|^2 \right|^2 \\ \text{subject to } |\tilde{z}_{(i)}|^2 = \eta \left(a_{(i)}^2 - b \right), \end{aligned} \quad (17)$$

where $\eta \in \mathbb{R}^{m^2}$ is a shrinkage parameter that accounts for the fact that $|\tilde{z}^{(\ell)}|^2$ is on average smaller than a^2 . This is because $\tilde{z}^{(\ell)}$ is obtained from a sequence of linear projections that reduce the overall norm. Since \tilde{z} is smaller, the solution to the off-set projection problem 17 is biased towards a larger offset. Introducing the shrinkage parameter η equal for every frame provides the flexibility to avoid this problem.

By solving for η first, we obtain the first and second order terms:

$$\eta^{(\ell)} = \frac{\sum_i d_{(i)} |\tilde{z}_{(i)}^{(\ell)}|^2}{\sum_i d_{(i)}^2}, \quad (18)$$

where $d_{(i)} = a_{(i)}^2 - b$. Solving for b for a fixed η gives

$$\begin{aligned} b^{(\ell)} - b^{(\ell-1)} &= \frac{1}{k} \sum_i \left(d_{(i)} - |\tilde{z}_{(i)}^{(\ell)}|^2 \frac{1}{\eta^{(\ell)}} \right) \\ &= \langle d_{(i)} \rangle - \frac{1}{\eta^{(\ell)}} \left\langle |\tilde{z}_{(i)}^{(\ell)}|^2 \right\rangle \\ &= \langle d_{(i)} \rangle - \frac{\langle d_{(i)}^2 \rangle \left\langle |\tilde{z}_{(i)}^{(\ell)}|^2 \right\rangle}{\left\langle d_{(i)} |\tilde{z}_{(i)}^{(\ell)}|^2 \right\rangle} \end{aligned}$$

To avoid strong perturbations, however, we set $\eta(\mathbf{q}) = .8$ if $\eta(\mathbf{q}) < 0.8$. When optimizing for a fluctuating offset ($b_{(i)}(\mathbf{q}) = b_{(i)}(0)$ constant for every frame), we simply replace the sum over i with the sum over \mathbf{q} . The update of z is then computed as a regular Fourier magnitude projection operator with an intensity offset:

$$\tilde{P}_{\mathcal{F}}^{(a_{(i)}^2 - b^{(\ell)})} \tilde{z}_{(i)}^{(\ell)} = \tilde{z}_{(i)}^{(\ell)} \sqrt{\frac{a_{(i)}^2 - b^{(\ell)}}{|\tilde{z}_{(i)}^{(\ell)}|^2}},$$

where we used the notation $\tilde{P} = \mathcal{F}P\mathcal{F}^*$.

In the following section we will show that common projection methods can recover the background even if the SNR is much smaller than 1.

VII. NUMERICAL TESTS

The object used to simulate the diffraction pattern is obtained from an SEM image of a cluster of commercial 50 nm colloidal gold spheres. The gray scale values

were converted to a sample thickness varying between 0 and 50 nm, and we assigned the complex index of refraction of a 750 eV x ray photon going through an organic compound (PMMA). Here the numerical tests are done assuming periodic boundary conditions. These boundary conditions ensure that every region of the object ψ is illuminated with an equal number of overlapping frames, in other words the null space of Q is empty. We use frames width of 16x16, probe width=8, step size =5, number of frames=8x8...64x64, RAAR algorithm, $\beta = .75$.

The error metrics $\varepsilon_F, \varepsilon_Q$ used to monitor progress are:

$$\|a\|_{\varepsilon_F}(\mathbf{z}^{(\ell)}) = \left\| [P_F - I] \mathbf{z}^{(\ell)} \right\|, \quad (19)$$

$$\|a\|_{\varepsilon_Q}(\mathbf{z}^{(\ell)}) = \left\| [P_Q - I] \mathbf{z}^{(\ell)} \right\|, \quad (20)$$

where I is the identity operator. This has to be compared to ε_0 , the error w.r.t the known solution:

$$\|a\|_{\varepsilon_0}(\mathbf{z}^{(\ell)}) = \min_{\varphi} \left\| e^{i\varphi} \mathbf{z}^{(\ell)} - \mathbf{Q}\hat{\psi} \right\| \quad (21)$$

where φ is an arbitrary global phase factor.

We report the following observations

- **Fluctuating intensities: (Fig. 4), (Intensity fluctuation in this tests are 20%)** By solving the new LSQ problem we obtain accelerated convergence and exact reconstructions every time we tested the problem, see (Fig. 4). No degradation (above numerical precision) introduced by intensities perturbed by 20%.
- **Scaling: (Fig. 5)** Improved convergence with larger problems. As we increase the number of frames, convergence slows down for standard projection operators (parameters: $m=16$, $Dx=4$, k varies, $n=k*Dx+m$)
- **Multiplexing: (Fig. 5)** Deconvolution of the incoherent sum of frames translated by 3 times the illuminating beam width.
- **Calibration: (Fig. 6).** Deconvolution of the incoherent sum of frames translated by 3 times the illuminating beam width, with unknown amplitude.
- **Positions: Fig. 7** Recovery of the positions perturbed by an unknown factor randomly distributed between ± 2.5 pixels.
- **Background: (Fig. 9), $\langle \|\mathbb{z}_{(i)}\| \rangle_i / \|b\| = 0.5$.** In Figure 8,9 we obtain exact reconstruction of the object and background (Background ratio $\|a\|/\|b\| = 10^{-6}$. Exact recovery (within numerical precision) was obtained with reduced step size $\delta x = 3r$. No degradation (above numerical precision) introduced by the background, nearly no influence on convergence rate.

# frames	clock time(s)	iteration	ε_0^2
standard			
4×4	0.7	121	<1e-11
8×8	1.4	125	<1e-11
16×16	4.9	144	<1e-11
24×24	26.3	400	4.3e-10
32×32	36.3	400	4.3e-4
48×48	90.7	400	3.4e-4
64×64	137.5	400	5.3e-3
augmented			
4×4	1.9	138	<1e-11
8×8	2.7	141	<1e-11
16×16	6.5	138	<1e-11
24×24	14	134	<1e-11
32×32	25.6	139	<1e-11
48×48	60.4	142	<1e-11
64×64	96.2	149	<1e-11

TABLE II: Performance of projection algorithms using matlab R2012a 64-bit (maci64) (lapack version 3.3.1, MKL 10.3.5) on 2x2.2GHz Quad-core Intel xeon using frames of dimension 16×16 .

The dominant computational effort at experimentally practical size scale ($k \ll n$) are the computation of frame-frame dot products and the linear solution of $H \setminus \mathbf{1}$. Each matrix entry $H_{i,j}$ requires computation of the norm or dot product of a pair of overlapping frames, each multiplied by the conjugate of the probe, normalized by $(\mathbf{Q}^* \mathbf{Q})^{-1}$ and translated by $\mathbf{x}_i - \mathbf{x}_{(j)}$. Since every frame has a fixed number of neighbors, this computation grows linearly with the number of frames k . Inversion of the $(k \times k)$ sparse matrix H , or the simple computation of $H^{-1} \mathbf{1}$ is typically a smaller computational problem than the computation of its entries.

CONCLUSIONS

The high redundancy in ptychographic data enables not only robust phase recovery but the recovery other parameters as well, such as the illuminating function itself¹⁷, position^{13,18}, coherence function¹⁶. Here we introduced a modified projection operator for the ptychographic reconstruction problem that accounts for fluctuating intensities, position errors, or poor calibration using multiplexing illumination, and an unknown offset (background) different for every pixel but constant throughout the acquisition (or vice versa).

By optimizing the phase among each frame, we solve the phase problem at a resolution given by the step size between frames. This intra-frame phase optimization may be applied to merge subregions reconstructed independently by distributed computer systems; For three dimensional objects, to merge two dimensional views re-

constructed independently into one three dimensional object. Finally, this intra-frame optimization could be applied to multi-scale reconstructions where frames are divided in regions of Fourier space.

The high redundancy in the data enables the identification of background fluctuations over $10^6 \times$ the signal and possibly more. We considered background fluctuations that are constant throughout a reduced dimension: either a flat offset that fluctuates for each snapshot, or an offset different for every pixel but constant throughout the acquisition. We introduced a parameter η that scales intensities along the reduced dimension in the optimization process that we found critical to achieve convergence.

Our implementation of the background noise subproblem optimization has negligible effect on clock time or memory footprint. The subproblem associated with fluctuating intensities increases the clock time per iteration but improves the convergence rate for large scale problems.

More work is needed to include other sources of noise, and to establish the optimal frequency of communication and the amount of overlap between sub-reconstruction regions.

ACKNOWLEDGMENTS

SM thanks Prof. Bin Yu for discussions on background and shrinkage. This work was supported by the Laboratory Directed Research and Development Program of Lawrence Berkeley National Laboratory under the U.S. Department of Energy contract number DE-

AC02-05CH11231 (C. Y., A. S., S. M.), and by the Director, Office of Science, Advanced Scientific Computing Research, of the U.S. Department of Energy under Contract No. DE-AC02-05CH11231 (F.M.). The computational results presented were obtained at the National Energy Research Scientific Computing Center (NERSC), which is supported by the Director, Office of Advanced Scientific Computing Research of the U.S. Department of Energy under contract number DE-AC02-05CH11232.

DISCLAIMERS

This document was prepared as an account of work sponsored by the United States Government. While this document is believed to contain correct information, neither the United States Government nor any agency thereof, nor the Regents of the University of California, nor any of their employees, makes any warranty, express or implied, or assumes any legal responsibility for the accuracy, completeness, or usefulness of any information, apparatus, product, or process disclosed, or represents that its use would not infringe privately owned rights. Reference herein to any specific commercial product, process, or service by its trade name, trademark, manufacturer, or otherwise, does not necessarily constitute or imply its endorsement, recommendation, or favoring by the United States Government or any agency thereof, or the Regents of the University of California. The views and opinions of authors expressed herein do not necessarily state or reflect those of the United States Government or any agency thereof or the Regents of the University of California.

Appendix A: Solution to the augmented problem

Here we set $\sum_{i=1}^k c_{(i)} = k$ and solve

$$\min_{\psi, c_{(i)}, \lambda} \mathcal{L}(\psi, c, \lambda), \text{ where } \mathcal{L} = \sum_i \|Q_{(i)}\psi - c_{(i)}z_{(i)}\|^2 + \lambda \left(\sum_i c_{(i)} - k \right), \quad (\text{A1})$$

where λ is a Lagrange multiplier. We could also set $c_1 = 1$ or any arbitrary number but numerical tests indicated improved performance of the former constraint. As we can see below, we can eliminate ψ in by block factorization and solve:

$$\arg \min_{c, \lambda} \|(I - P_{\mathbf{Q}})\text{Diag}(c)\mathbf{z}\|^2 + \lambda \left(\sum c_i - k \right).$$

We note that $c_{(i)} \in \mathbb{C}$ are complex. To find the coefficients $c_{(i)}$, we use the normal equation associated with the LSQ problem (Eq. A1) :

$$\begin{pmatrix} \sum_i Q_{(i)}^* Q_{(i)} & -Q_1^* z_1 & \dots & \dots & -Q_k^* z_k & 0 \\ -z_1^* Q_1 & z_1^* z_1 & 0 & \dots & 0 & 1 \\ \vdots & 0 & \ddots & & \vdots & \vdots \\ \vdots & \vdots & & & 0 & \vdots \\ -z_k^* Q_k & 0 & \dots & 0 & z_k^* z_k & 1 \\ 0 & 1 & \dots & & 1 & 0 \end{pmatrix} \begin{pmatrix} \psi \\ c_1 \\ \vdots \\ c_k \\ \lambda \end{pmatrix} = \begin{pmatrix} 0 \\ 0 \\ \vdots \\ 0 \\ k \end{pmatrix}.$$

We can partition the equation above as

$$\begin{pmatrix} A & B^* \\ B & D \end{pmatrix} \begin{pmatrix} \psi \\ \mathbf{c} \\ \lambda \end{pmatrix} = \begin{pmatrix} 0 \\ 0 \\ k \end{pmatrix},$$

where

$$A = \sum_{i=1}^k Q_{(i)}^* Q_{(i)}, \quad B = \begin{pmatrix} -z_1^* Q_1 \\ \vdots \\ -z_k^* Q_k \\ 0 \end{pmatrix}, \quad D = \begin{pmatrix} z_1^* z_1 & 0 & \dots & 0 & 1 \\ 0 & z_1^* z_1 & \ddots & \vdots & \vdots \\ \vdots & \ddots & \ddots & 0 & \vdots \\ 0 & \dots & 0 & z_k^* z_k & 1 \\ 1 & \dots & \dots & 1 & 0 \end{pmatrix}, \quad \mathbf{c} = \begin{pmatrix} c_1 \\ \vdots \\ c_k \end{pmatrix}$$

Using the block factorization

$$\begin{pmatrix} I & 0 \\ BA^{-1} & I \end{pmatrix} \begin{pmatrix} A & B^* \\ 0 & D - BA^{-1}B^* \end{pmatrix} \begin{pmatrix} \psi \\ \mathbf{c} \\ \lambda \end{pmatrix} = \begin{pmatrix} 0 \\ 0 \\ k \end{pmatrix},$$

We obtain:

$$(D - BA^{-1}B^*) \begin{pmatrix} \mathbf{c} \\ \lambda \end{pmatrix} = \begin{pmatrix} 0 \\ k \end{pmatrix} \quad (\text{A2})$$

We can express the Schur complement:

$$D - BA^{-1}B^* = \begin{pmatrix} H & \mathbf{1} \\ \mathbf{1}^* & 0 \end{pmatrix}, \quad \mathbf{1} = \begin{pmatrix} 1 \\ \vdots \\ 1 \end{pmatrix}$$

where

$$H_{i,j} = z_{(i)}^* \left(\delta_{i,j} I - Q_{(i)} \left(\sum_{(l)} Q_{(l)}^* Q_{(l)} \right)^{-1} Q_{(j)}^* \right) z_{(j)}.$$

Note: $H\mathbf{c} = \nabla_{\mathbf{c}} \|(I - P_Q)\mathbf{z} \text{Diag}(\mathbf{c})\|^2$

By block-wise inversion, of Eq. A2 we obtain \mathbf{c} and the scaling factor λ from a sparse linear equation:

$$H\mathbf{c} = -\lambda\mathbf{1}, \quad -\lambda = (\mathbf{1}^* H^{-1} \mathbf{1})^{-1} k$$

Appendix B: Taylor expansion

We consider the case in which the probe w is translated from the input coordinate by an unknown distance ξ . We call \mathbf{Q}_ξ the unknown illumination matrix used to generate the data. To determine the illumination matrix, we determine the parameter ξ so that the error $\varepsilon_{\mathbf{Q}_\xi}$ is minimized:

$$\arg \min_{\xi} \left\| [I - P_{\mathbf{Q}_\xi}] \mathbf{z} \right\|^2 \quad (\text{B1})$$

We restrict initially to 1-dimensional translations. Given the illumination function w , we can compute the first and second order derivatives with respect to translation. We denote by Q_i, R_i, S_i the illumination matrices that extract a frame out of an image and multiplies by $(w(\mathbf{x}), \partial_x w(\mathbf{x}), \partial_x^2 w(\mathbf{x}))$ respectively. $\mathbf{Q}, \mathbf{R}, \mathbf{S}$ are tall and skinny matrices of the same size as \mathbf{Q} discussed earlier, with identical location of the non-zero entries. The probe is perturbed to second order as follows:

$$\mathbf{Q}_\xi = \mathbf{Q} + \xi \mathbf{R} + \xi^2 \mathbf{S}.$$

where ξ is diagonal and real, and represents the translation distance different for every frame i . We minimize

$$\arg \min_{\xi} \left\| \left[I - (\mathbf{Q} + \xi \mathbf{R} + \xi^2 \mathbf{S}) \left[(\mathbf{Q} + \xi \mathbf{R} + \xi^2 \mathbf{S})^* (\mathbf{Q} + \xi \mathbf{R} + \xi^2 \mathbf{S}) \right]^{-1} (\mathbf{Q} + \xi \mathbf{R} + \xi^2 \mathbf{S})^* \right] \mathbf{z} \right\|^2 \quad (\text{B2})$$

By Taylor expansion:

$$[\cdot]^{-1} \simeq \frac{1}{\mathbf{Q}^* \mathbf{Q}} \left(1 - (\mathbf{R}^* \xi \mathbf{Q} + \mathbf{Q}^* \xi \mathbf{R} + O(\xi^2)) \frac{1}{\mathbf{Q}^* \mathbf{Q}} \right)$$

the term $O(\xi^2)$ includes other second order terms that we will not need. We write the expansion of the residual in Eq. (B1) $f_0 + f_1(\xi) + f_2(\xi^2)$ as:

$$f_0 = [I - P_{\mathbf{Q}}] \mathbf{z} \equiv \underline{\mathbf{z}} \quad (\text{B3})$$

We define $\phi^* \equiv \frac{1}{\mathbf{Q}^* \mathbf{Q}} \mathbf{Q}^*$, and express the first order as

$$f_1 = [-\xi \mathbf{R} \phi^* - \phi \mathbf{R}^* \xi + \phi (\mathbf{R}^* \xi \mathbf{Q} + \mathbf{Q}^* \xi \mathbf{R}) \phi^*] \mathbf{z}$$

by defining $\mathbf{z}_{\mathbf{R}} \equiv \mathbf{R} \phi^* \mathbf{z}$, using $P_{\mathbf{Q}} = \mathbf{Q} \phi^* = \phi \mathbf{Q}^*$, and rearranging:

$$\begin{aligned} f_1 &= -\xi \mathbf{z}_{\mathbf{R}} - \phi \mathbf{R}^* \xi (\mathbf{z} - \mathbf{Q} \phi^* \mathbf{z}) + \phi \mathbf{Q}^* \xi \mathbf{z}_{\mathbf{R}} \\ &= -(1 - P_{\mathbf{Q}}) \xi \mathbf{z}_{\mathbf{R}} - \phi \mathbf{R}^* \xi \mathbf{z} \end{aligned} \quad (\text{B4})$$

using the equality $\underline{\mathbf{z}}(I - P_{\mathbf{Q}}) = \underline{\mathbf{z}}$, setting $O_{\mathbf{R}} \equiv \mathbf{R} \phi^* \phi \mathbf{R}^* = \mathbf{R} \frac{1}{\mathbf{Q}^* \mathbf{Q}} \mathbf{R}^*$ and rearranging we obtain:

$$\begin{aligned} f_2 &= - \left[\xi \mathbf{R} \frac{1}{\mathbf{Q}^* \mathbf{Q}} \mathbf{R}^* \xi + \xi^2 \mathbf{S} \phi + \mathbf{Q} O(\xi^2) \right] \mathbf{z} \\ &= -\xi O_{\mathbf{R}} \xi \mathbf{z} - \xi^2 \mathbf{z}_{\mathbf{S}} + \mathbf{Q} O(\xi^2) \mathbf{z} \end{aligned} \quad (\text{B5})$$

where $\mathbf{z}_{\mathbf{S}} \equiv \mathbf{S} \phi^* \mathbf{z}$. We rewrite Eq. (B1) above as:

$$\left\| [I - P_{\mathbf{Q}_\xi}] \mathbf{z} \right\|^2 = f_0^* f_0 + f_0^* f_1 + f_1^* f_0 + f_1^* f_1 + f_0^* f_2 + f_2^* f_0 + O(\xi^3)$$

we note that $\underline{\mathbf{z}}^* \mathbf{Q} = \underline{\mathbf{z}}^* \phi = 0$, set $\mathbf{z}_{\mathbf{Q}} \equiv \mathbf{Q} \phi \mathbf{z}$ and obtain the first and second order terms of Eq. (B1):

$$\begin{aligned} f_0^* f_1 + f_1^* f_0 &= -\underline{\mathbf{z}}^* \xi \mathbf{z}_{\mathbf{R}}, -\mathbf{z}_{\mathbf{R}}^* \xi \underline{\mathbf{z}} \\ f_1^* f_1 + f_0^* f_2 + f_2^* f_0 &= \mathbf{z}_{\mathbf{R}}^* \xi (I - P_{\mathbf{Q}}) \xi \mathbf{z}_{\mathbf{R}} + \underline{\mathbf{z}} \xi O_{\mathbf{R}} \xi \underline{\mathbf{z}} - \underline{\mathbf{z}}^* \xi O_{\mathbf{R}} \xi \mathbf{z} - \mathbf{z}^* \xi^2 \mathbf{z}_{\mathbf{S}} - \mathbf{z}^* \xi O_{\mathbf{R}} \xi \underline{\mathbf{z}} - \mathbf{z}_{\mathbf{S}}^* \xi^2 \underline{\mathbf{z}}, \\ &= \mathbf{z}_{\mathbf{R}}^* \xi^2 \mathbf{z}_{\mathbf{R}} - \underline{\mathbf{z}}^* \xi^2 \mathbf{z}_{\mathbf{S}} - \mathbf{z}_{\mathbf{S}}^* \xi^2 \underline{\mathbf{z}} - \mathbf{z}^* \xi O_{\mathbf{R}} \xi \mathbf{z} + \mathbf{z}_{\mathbf{Q}}^* \xi O_{\mathbf{R}} \xi \mathbf{z}_{\mathbf{Q}} - \mathbf{z}_{\mathbf{R}}^* P_{\mathbf{Q}} \xi \mathbf{z}_{\mathbf{R}}. \end{aligned} \quad (\text{B6})$$

By using the definition of $\mathbf{z}_{\mathbf{Q}}, \mathbf{z}_{\mathbf{R}}, P_{\mathbf{Q}}$ and $O_{\mathbf{R}}$ it is easy to show that $\mathbf{z}_{\mathbf{Q}}^* \xi O_{\mathbf{R}} \xi \mathbf{z}_{\mathbf{Q}} = \mathbf{z}_{\mathbf{R}}^* \xi P_{\mathbf{Q}} \xi \mathbf{z}_{\mathbf{R}}$ and simplify as:

$$f_1^* f_1 + f_0^* f_2 + f_2^* f_0 = \mathbf{z}_{\mathbf{R}}^* \xi^2 \mathbf{z}_{\mathbf{R}} - \underline{\mathbf{z}}^* \xi^2 \mathbf{z}_{\mathbf{S}} - \mathbf{z}_{\mathbf{S}}^* \xi^2 \underline{\mathbf{z}} - \mathbf{z}^* \xi O_{\mathbf{R}} \xi \mathbf{z}, \quad (\text{B7})$$

$$\simeq \mathbf{z}_{\mathbf{R}}^* \xi^2 \mathbf{z}_{\mathbf{R}} - \mathbf{z}^* \xi O_{\mathbf{R}} \xi \mathbf{z}. \quad (\text{B8})$$

We note that $-\underline{\mathbf{z}}^* \xi^2 \mathbf{z}_{\mathbf{S}} - \mathbf{z}_{\mathbf{S}}^* \xi^2 \underline{\mathbf{z}}$ is a second order correction if we assume that \mathbf{z} is in that range of an unknown \mathbf{Q}_ξ for small ξ . By setting $\partial_{\xi_i} \|\cdot\|^2 = 0$, we obtain the linear equation:

$$\sum_j \left(2 (\mathbf{z}_{\mathbf{R}_i}^* \mathbf{z}_{\mathbf{R}_i} - \underline{\mathbf{z}}_i^* \mathbf{z}_{\mathbf{S}_i} - \mathbf{z}_{\mathbf{S}_i}^* \underline{\mathbf{z}}_i) \delta_{ij} - \mathbf{z}_i^* O_{\mathbf{R}_{ij}} \mathbf{z}_j - \mathbf{z}_j^* O_{\mathbf{R}_{ji}} \mathbf{z}_i \right) \xi_j = \mathbf{z}_i^* \mathbf{z}_{\mathbf{R}_i} + \mathbf{z}_{\mathbf{R}_i}^* \underline{\mathbf{z}}_i$$

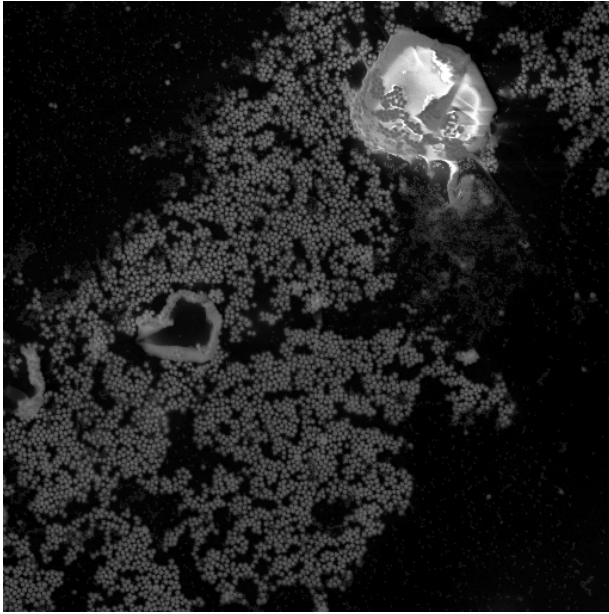


FIG. 2: object ψ used to simulate diffraction data)

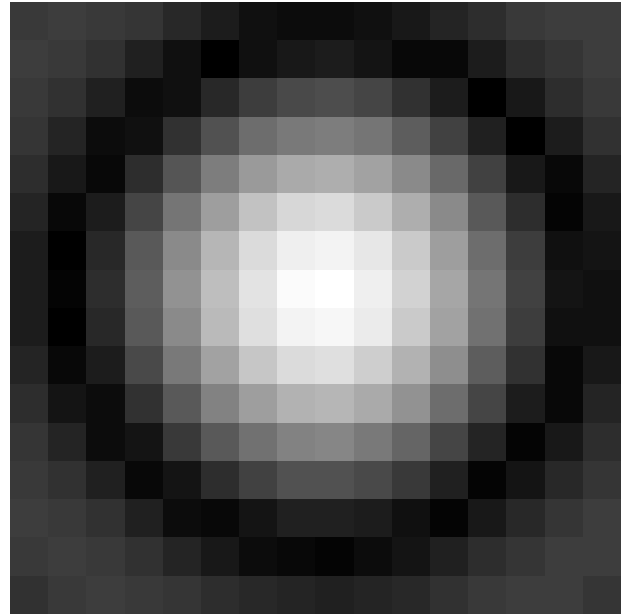


FIG. 3: Absolute value of the probe $|w(\mathbf{r})|$ used in simulations (16×16 pixels)

* smarchesini@lbl.gov

† cyang@lbl.gov

‡ frmaia@lbl.gov

- ¹ J. M. Rodenburg and R. H. T. Bates. The theory of super-resolution electron microscopy via wigner-distribution deconvolution. *Phil. Trans. R. Soc. Lond. A*, 339:521–553, 1992.
- ² H N Chapman. Phase-retrieval x-ray microscopy by wigner-distribution deconvolution. *Ultramicroscopy*, 66:153–172, 1996.
- ³ H. M. L. Faulkner and J. M. Rodenburg. Movable aperture lensless transmission microscopy: a novel phase retrieval algorithm. *Phy. Rev. Lett.*, 93:023903, 2004.
- ⁴ J. M. Rodenburg and H. M. L. Faulkner. A phase retrieval algorithm for shifting illumination. *Appl. Phy. Lett.*, 85:4795–4797, 2004.
- ⁵ Pierre Thibault, Martin Dierolf, Andreas Menzel, Oliver Bunk, Christian David, and Franz Pfeiffer. High-Resolution scanning x-ray diffraction microscopy. *Science*, 321(5887):379–382, 2008.
- ⁶ Martin Dierolf, Andreas Menzel, Pierre Thibault, Philipp Schneider, Cameron M. Kewish, Roger Wepf, Oliver Bunk, and Franz Pfeiffer. Ptychographic x-ray computed tomography at the nanoscale. *Nature*, 467:436–439, 2011.
- ⁷ Z. Wen, C. Yang, X. Liu, and S. Marchesini. Alternating direction methods for classical and ptychographic phase retrieval. *Technical Report*, 2012.
- ⁸ C. Yang, J. Qian, A. Schirotzek, F. Maia, and S. Marchesini. Iterative algorithms for ptychographic phase retrieval. *Technical Report LBNL-4598E*, 2011, 1105.5628.
- ⁹ P Thibault and M Guizar-Sicairos. Maximum-likelihood refinement for coherent diffractive imaging. *New Journal of Physics*, 14(6):063004, 2012.
- ¹⁰ E. J. Candes, T. Strohmer, and V. Voroninski. PhaseLift: Exact and Stable Signal Recovery from Magnitude Measurements via Convex Programming. *Communications on Pure and Applied Mathematics*, 1109.4499.
- ¹¹ H. Ohlsson, A. Y. Yang, R. Dong, and S. Shankar Sastry. Compressive Phase Retrieval From Squared Output Measurements Via Semidefinite Programming. November 2011, 1111.6323.
- ¹² E. J. Candes, Y. Eldar, T. Strohmer, and V. Voroninski. Phase Retrieval via Matrix Completion. *ArXiv e-prints*, September 2011, 1109.0573.
- ¹³ M. Guizar-Sicairos and J. R. Fineup. Phase retrieval with transverse translation diversity: a nonlinear optimization approach. *Opt. Express*, 16:7264–7278, 2008.
- ¹⁴ R. Luke. Relaxed averaged alternating reflections for diffraction imaging. *Inverse Problems*, 21:37–50, 2005.
- ¹⁵ J. R. Fienup. Phase retrieval algorithms: a comparison. *Appl. Opt.*, 21:2758–2769, 1982.
- ¹⁶ Jesse N. Clark and Andrew G. Peele. Simultaneous sample and spatial coherence characterisation using diffractive imaging. *Applied Physics Letters*, 99(15):154103, 2011.
- ¹⁷ P. Thibault, M. Dierolf, O. Bunk, A. Menzel, and F. Pfeiffer. Probe retrieval in ptychographic coherent diffractive imaging. *Ultramicroscopy*, 109:338–343, 2009.

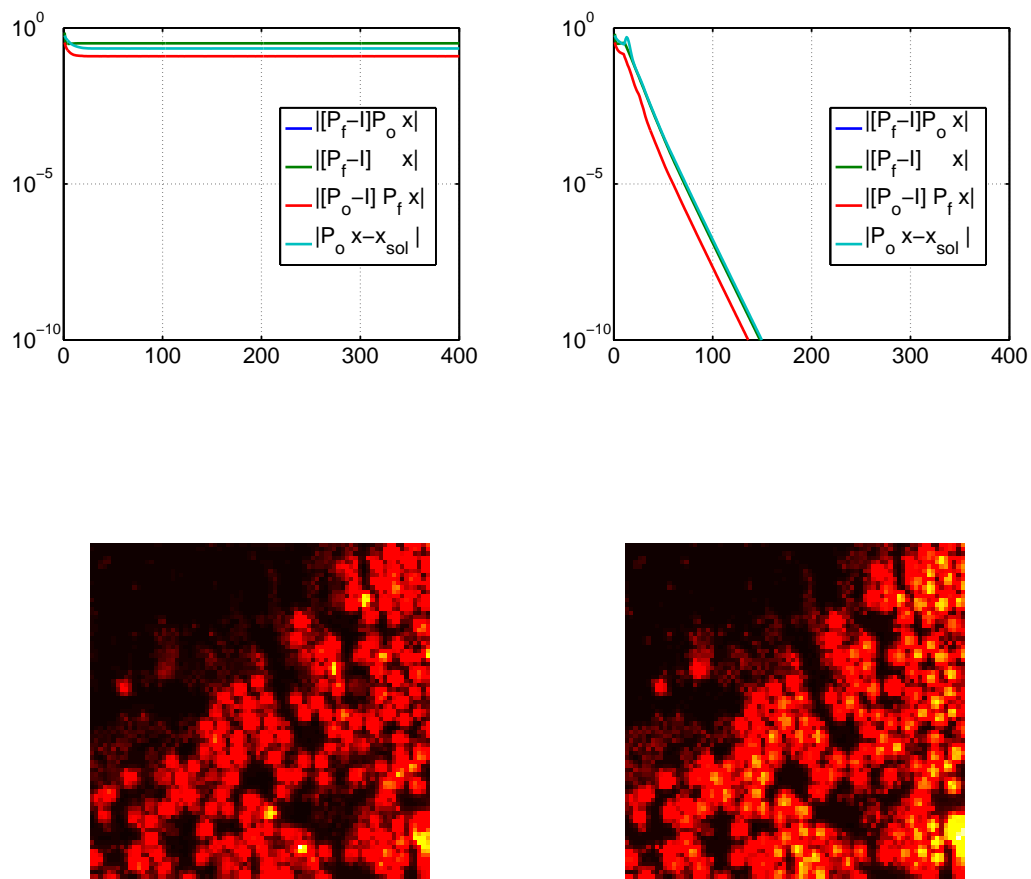
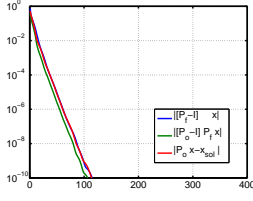
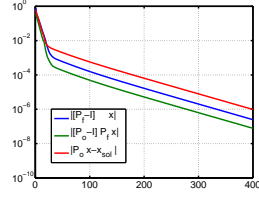


FIG. 4: Convergence rate with an I0-error of $\pm 20\%$. (left) old projection operator (right) new projection operator. (bottom) reconstruction from data with I0-error, and solution (reconstruction using the new projection operator is within the computer numerical precision).

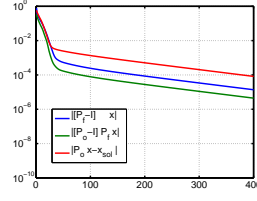
¹⁸ A.M. Maiden, M.J. Humphry, M.C. Sarahan, B. Kraus, and J.M. Rodenburg. An annealing algorithm to correct positioning errors in ptychography. *Ultramicroscopy*, 120(0):64 – 72, 2012.



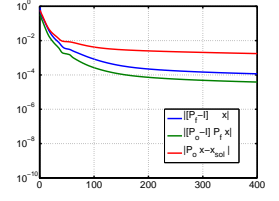
(a) 8×8 frames



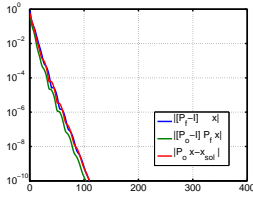
(b) 16×16 frames



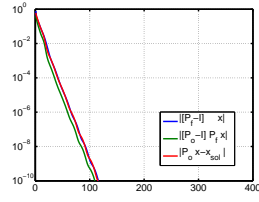
(c) 32×32 frames



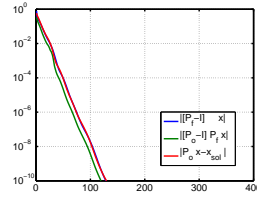
(d) 64×64 frames



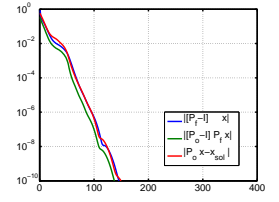
(e) 8×8 frames



(f) 16×16 frames



(g) 32×32 frames



(h) 64×64 frames

FIG. 5: Convergence rate (ε_F , ε_Q , ε_0 vs number of iteration ℓ) for (top) regular reconstruction. (bottom) using augmented projection ($m = 16$ and step size $x_1 - x_2 = 3$)

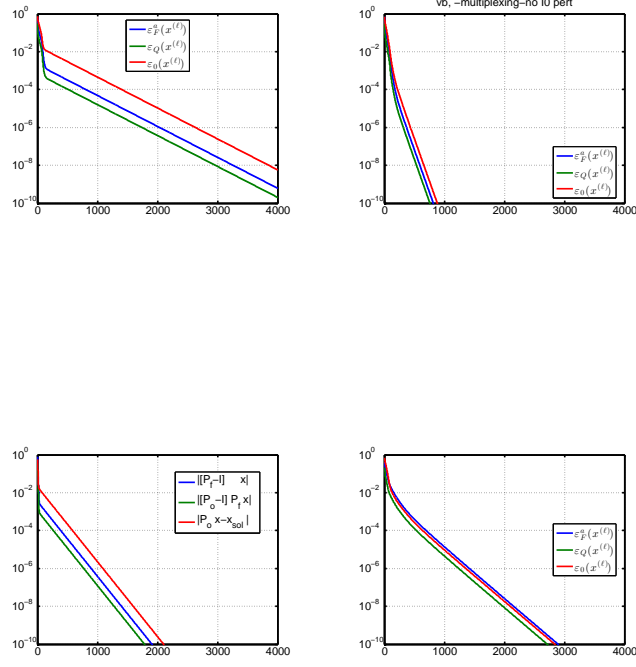


FIG. 6: Convergence rate with incoherent illumination of 4 beams, separated by $3 \times$ the probe width (FWHM) using standard projection algorithms (top left), with intermediate phase optimization (top-right), phase and amplitude (bottom-left), and phase and amplitude with initial amplitude error of 20% (bottom right), frame width 16×16 , 16×16 frames, step size 3.5 pixels close packing with ± 1 pixel known random perturbations.

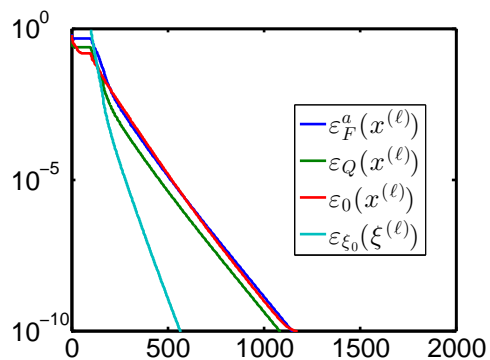


FIG. 7: Reconstruction with position errors using the method described in section V, where $\varepsilon_{\xi_0} = \|\xi - \xi_0\|/\|\xi_0\|$, and the perturbations in position are randomly distributed with $\langle \xi_0 \rangle = \frac{1}{k} \sum_i \|\xi_i\| = 2.5$ resolution elements. (number of frames: 16×16 , frame dimensions 32×32 , step size: 3.5 pixels, hexagonal packing with known random perturbations of ± 1 pixels and unknown ξ random perturbations).

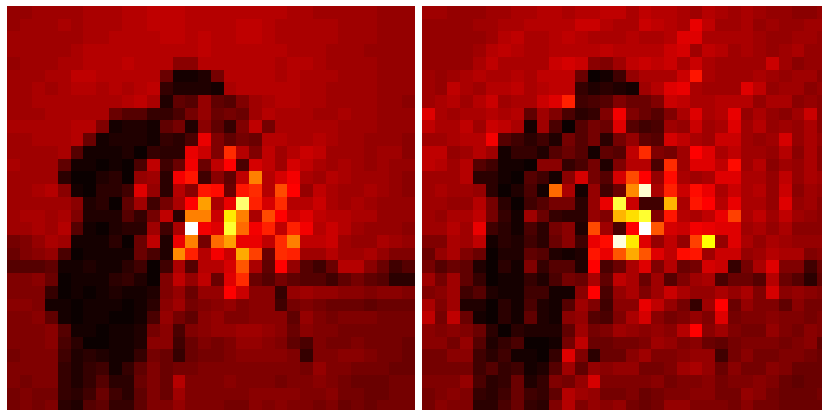


FIG. 8: Two measured intensities with additive background (SNR=0.5). In a separate test the diffraction data was buried by the background ((in other figures not included background was $10^6 \times$ the signal).

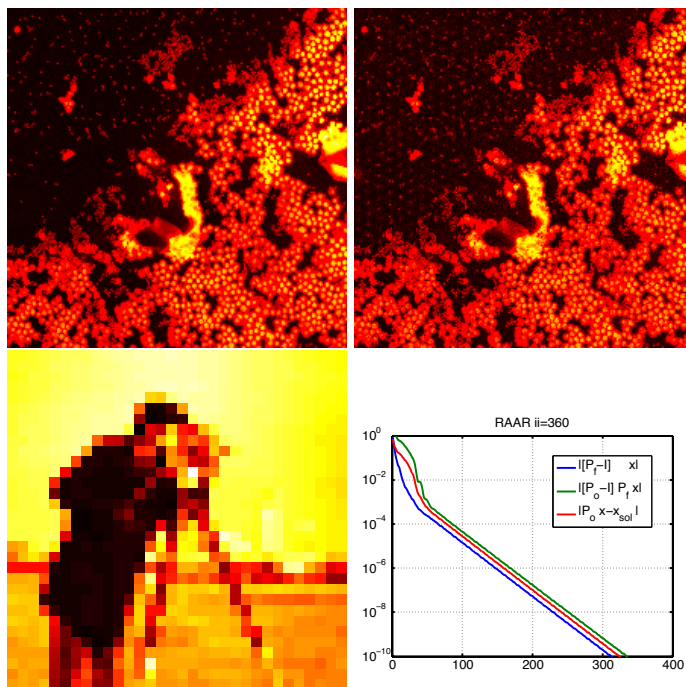


FIG. 9: (top) reconstructed image with background optimization (left) and without (right). (bottom) reconstructed background (left), convergence behavior(right)